Electronic version of an article published as International Journal of Bifurcation and Chaos Vol. 14, No. 4, 2004, 1305-1324,
DOI: 10.1142/S0218127404009983 © World Scientific Publishing Company, https://www.worldscientific.com/worldscinet/ijbc

Bifurcation and Chaos in Coupled BVP Oscillators

Tetsushi Ueta [*], Hisayo Miyazaki [†], Takuji Kousaka [‡], and Hiroshi Kawakami [§]

Abstract

Bonhöffer-van der Pol(BVP) oscillator is one of classic model exhibiting typical nonlinear phenomena in the planar autonomous system. This paper gives an analysis of equilibria, periodic solutions, strange attractors of two BVP oscillators coupled by a resister. When an oscillator is fixed its parameter values in non-oscillatory region and the other is in oscillatory regin, then the double scroll attractor is emerged by the coupling. Bifurcation diagrams are obtained numerically from the mathematical model and chaotic parameter regions are clarified. We also confirm the existence of period-doubling cascades and chaotic attractors in experimental laboratory.

1 Notation

d**:** pitchfork bifurcation of an equilibrium

h**:** Hopf bifurcation of an equilibrium

G**:** tangent bifurcation of a limit cycle

I^k**:** period-doubling bifurcation of a k-periodic limit cycle

NS**:** Neimark-Sacker bifurcation of a limit cycle

Pf**:** pitchfork bifurcation of a limit cycle

If these symbols have a subscript, it means only an index number.

2 Introduction

At the first time, BVP (Bonhöffer van der Pol) equation has been derived as a simplified model of Hodkin-Huxley equation by FitzHugh and Nagumo [FitzHugh, 1961][Nagumo, 1962]. They reduce the Hodkin-Huxley equation (four-dimensional) to a two-dimensional system called the BVP equation or FitzHugh-Nagumo model by extracting excitability of the dynamics in Hodkin-Huxley equation[Rocsoreanu *et al.*, 2000]. It can be regarded as a reasonable extension of van der Pol equation, in fact, the BVP equation can be realized by a circuitry by using simple passive elements and one nonlinear conductor. Nowadays the BVP equation becomes one of classic nonlinear oscillator models.

To explain mutual synchronization phenomena in biological activities, the BVP oscillator is often used as a fundamental oscillatory unit because of its simple structure. A complete topological and qualitative investigation of the BVP equation with a cubic nonlinearity has been done by Bautin[Bautin, 1975]. Kitajima also studied same system[Kitajima *et al.*, 1998] and showed bifurcation diagrams of equilibria. A

[*]Center for Advanced Information Technology, Tokushima University, Japan
[†]Dept. Information Science and Intelligent Systems, Tokushima University, Japan
[‡]Dept. Electronics and Electrical Engineering, Fukuyama University, Japan
[§]Dept. Electrical and Electronics Engineering, Tokushima University, Japan

rich variety of nonlinear phenomenon is observed compared with van der Pol equation. A hard oscillation, separatrix loops, bifurcations for equilibria and limit cycles are occurred.

While, mutually coupled oscillators have been studied for three decades, as an analog model in order to simulate other large-scaled dynamical systems; physical, biological and chemical activities. Many impressive results about coupled van der Pol oscillators are clarified for now[Linkens, 1974][Endo *et al.*, 1978]. Synchronizing phenomena, e.g., in-phase, anti-phase, or n-phase synchronization are analyzed and rigorously proven. Also BVP is a good oscillating unit for a coupling system, since it is second-dimensional, simple, and robust.

As applications of the BVP equation under above background, Hoque[Hoque *et al.*, 1995] clarified synchronization of the resistively coupled BVP oscillators, and Papy[Papy *et al.*, 1995][Papy *et al.*, 1996] studied bifurcation structure of them. Lately Tsumoto et al. reported burst responses in the modified BVP oscillator[Tsumoto *et al.*, 1999]. They focused only on the behavior of the coupled system consisting of 'identical' oscillators (all oscillators have same parameter values). It enables us to analyze the system in symmetry point of view by using group theory. However, no circuit experiments have been shown.

In this paper, we investigate the resistively coupled BVP oscillators. We focus our eyes on 'unbalanced' situation in the coupled system, namely, two BVP oscillators are coupled, and each of them has different value of the internal impedance. Then we found an odd shape of chaotic attractor like a double scroll attractor[Chua *et al.*, 1986][Chua, 1993] after the period-doubling bifurcation cascade. These results points out that unbalanced coupling oscillators rather have a rich variety of nonlinear phenomena with a reasonable parameter range.

Firstly we formulate single BVP oscillator with a saturation characteristic. The nonlinear characteristics is modeled from experimental measurement of an FET. Some dynamical properties of the oscillator are given. Next, we investigate bifurcations of equilibria and periodic solutions in the resistively coupled BVP oscillators. Bifurcation diagrams are obtained by numerical methods, and corresponding phenomena are confirmed in both numerical simulation and laboratory experiments. We conclude that chaotic solutions are obtained via period-doubling bifurcation cascades.

3 Properties of Single BVP Oscillator

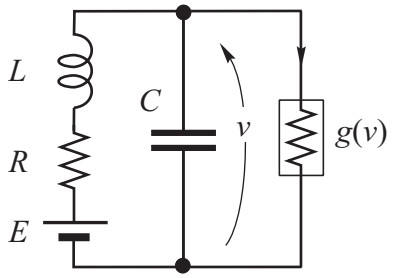

Figure 1: BVP oscillator

Firstly we describe dynamical behavior of single BVP oscillator with a nonlinear conductor modeled from a real electronic device.

3.1 Circuit Model

Figure 1 shows the original BVP oscillator. The circuit equations is given as:

$$\begin{aligned} C\frac{dv}{dt} &= -i - g(v) \\ L\frac{di}{dt} &= v - ri + E \end{aligned} \tag{1}$$

Assume that $g(v)$ has odd function characteristics, and neglect E for convenience sake. Then Eq.(1) has a permutation $(v, i) \to (-v, -i)$, and the direct voltage source E is often used for destroying the symmetry property of the system to avoid degeneracy.

3.2 Implementation of $g(v)$ by using an FET

As a nonlinear conductor $g(v)$, we choose a 2SK30A FET. This transistor is not special, but widely used for industrial fields. It is driven negatively by using an op-amp inverter shown in Fig. 2.

We approximate the nonlinear conductance by a negative saturation function:

$$g(v) = -a \tanh bv. \tag{2}$$

The Marquardt-Levenberg method (nonlinear least square method) is applied to fit this data, then $a = 6.89099 \times 10^{-3}$ and $b = 0.352356$ are obtained. Figure 3 shows a measured v-i characteristics from laboratory experiments of the FET, and the numerical value of the negative saturation function, and their difference. It is obvious that the approximation is reasonably sufficient.

In the original BVP equation, $g(v)$ is described by a third order polynomial. While, we simply assume the sigmoidal function Eq. (2) for experimental measurements from the FET, and consistently use it through this paper. However, this assumption is reasonable since dynamic range of v in the coupled system with Eq. (2) is almost restricted within the third-power term region. Appendix 4.7 briefly mentions the coupled system with third-power terms.

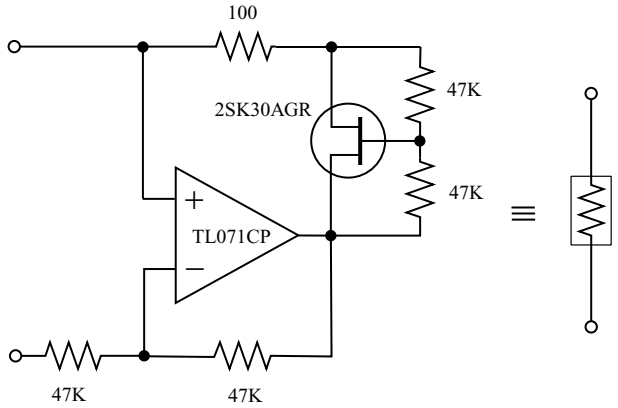

Figure 2: A nonlinear conductor.

Equation (1) can be rewritten as follows:

$$\begin{aligned} \dot{x} &= -y + \tanh \gamma x \\ \dot{y} &= x - ky. \end{aligned} \tag{3}$$

where,

$$\cdot = d/d\tau, \quad x = \sqrt{\frac{C}{L}}v, \quad y = \frac{i}{a} \tag{4}$$

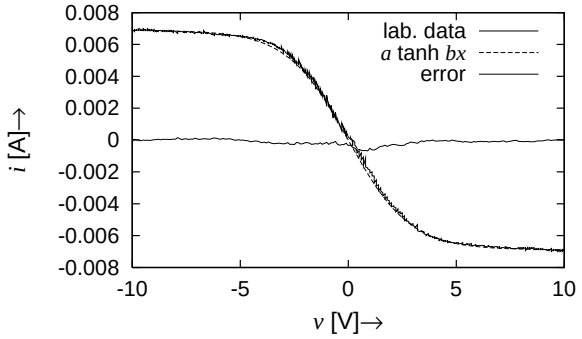

Figure 3: Measurement data of the FET, its approximation by $\tan bv$, and the error between them.

and

$$\tau = \frac{1}{\sqrt{LC}}t, \quad k = r\sqrt{\frac{C}{L}}, \quad \gamma = ab\sqrt{\frac{L}{C}} \tag{5}$$

3.3 Bifurcations in Single BVP Oscillator

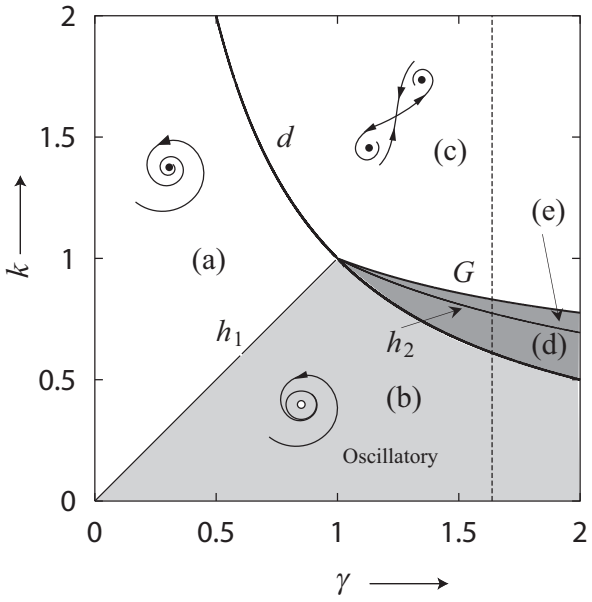

Figure 4: Bifurcation diagram of equilibria in Eq.(3)

Figure 4 shows bifurcation diagram of Eq. (3) in γ-k plane. Basically at least three equilibria are generated in this system, and they are changed their stability by bifurcation.

In area (a), there exist a sink at the origin O. d is pitchfork bifurcation of O and this bifurcation curve is given by $k = \gamma^{-1}$. As the parameter varies from area (a) to (c), a sink origin is changed to a saddle origin, and two sinks $C^+ = (x_c, y_c)$ and $C^- = (-x_c, -y_c)$ are generated.

h_1 shows the super critical Hopf bifurcation set for the origin and it is given by $k = \gamma$, $0 \leq \gamma \leq 1$. As the parameter varies from area (a) to (b), the sink is changed to a source and a stable limit cycle is obtained. While, as the parameter varies from area (b) to (d), a source origin is bifurcated into a saddle origin and two sources C^+ and C^-.

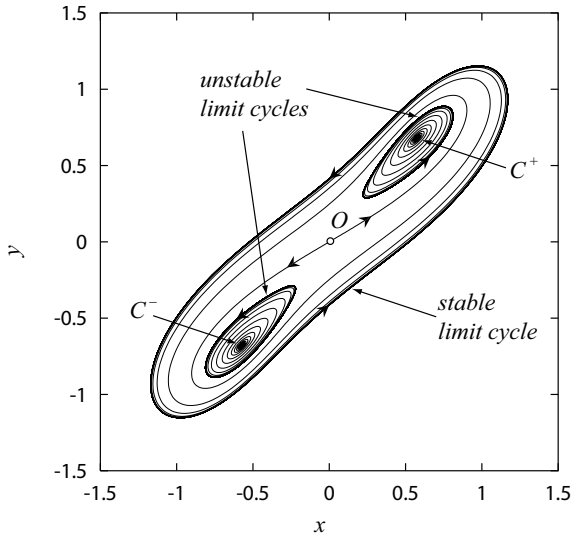

Figure 5: Phase portrait of the system (3). $k = 0.707(r = 475\ [\Omega])$. There exist two sinks, saddle, two unstable limit cycles, and a stable limit cycle.

h_2 is the sub-critical Hopf bifurcation for sinks, thus, as the parameter changes from area (d) to (e), source C^+ and C^- become sinks, and subsequently two unstable limit cycles are generated.

Inside area (e), two unstable limit cycles are knitted together and forms two separatrix loops.

Finally, as the parameter changes from area (e) to (c), stable and unstable limit cycles are disappeared together by the tangent bifurcation G.

As a summary, the areas sectioned by bifurcation curves are classified as follows:

(a) : a sink

(b) : a source and a stable limit cycle

(c) : a saddle and two sinks

(d) : two sinks, a saddle, one or two unstable limit cycles, one stable limit cycle

(e) : two sources, a saddle, a stable limit cycle

Note that there exists a separatrix loop in area (e), i.e., the saddle and two unstable limit cycles are knitted together by this bifurcation. Figure 5 shows phase portraits of the system (3) according to the area (d) in Fig.4. It is a hard oscillation. Two unstable limit cycles are generated by a sub-critical Hopf bifurcation h_2 in Fig. 4.

We consistently use the following parameters thorough this paper:

$$L = 10\ [\mathrm{mH}], \quad C = 0.022\ [\mu\mathrm{F}] \tag{6}$$

thus we have

$$\sqrt{\frac{L}{C}} = 674.2, \quad \gamma = 1.637. \tag{7}$$

This value of γ is indicated as a dash line in Fig. 4. Therefore we always obtain at least two attractors in the phase plane.

4 Resistively Coupled BVP Oscillators

The simplest implementation of the diffusively coupling in electric circuits is a register. Some biological activities can be interpreted by resistively coupled oscillators. In this section, we investigate dynamical properties of diffusively coupled 'unbalanced' oscillators.

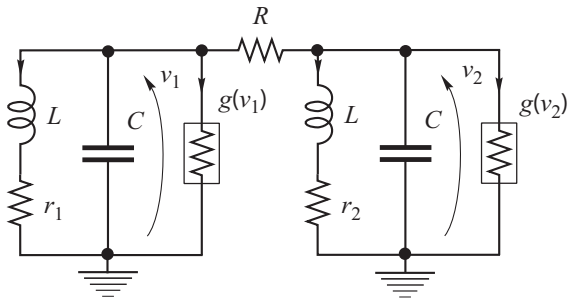

Figure 6: Coupled BVP oscillators

4.1 Circuit Model

BVP oscillators coupled by a register is shown in Fig. 6. Let $G = 1/R$. Then the circuit equations are derived as follows:

$$\begin{aligned} C\frac{dv_1}{dt} &= -i_1 + a\tanh bv_1 - G(v_1 - v_2) \\ L\frac{di_1}{dt} &= v_1 - ri_1 \\ C\frac{dv_2}{dt} &= -i_2 + a\tanh bv_2 - G(v_2 - v_1) \\ L\frac{di_2}{dt} &= v_2 - ri_2 \end{aligned} \tag{8}$$

By using scaled variables Eqs.(5), and let

$$x_j = \sqrt{\frac{C}{L}}v_j, \quad y_j = \frac{i_j}{a}, \quad k_j = r_j\sqrt{\frac{C}{L}}, \qquad j = 1, 2. \tag{9}$$

$$\tau = \frac{1}{\sqrt{LC}}t, \quad \gamma = ab\sqrt{\frac{L}{C}} \quad \delta = \sqrt{\frac{L}{C}}G. \tag{10}$$

Finally we have a normalized equation:

$$\begin{aligned} \dot{x}_1 &= -y_1 + \tanh\gamma x_1 - \delta(x_1 - x_2) \\ \dot{y}_1 &= x_1 - k_1 y_1 \\ \dot{x}_2 &= -y_2 + \tanh\gamma x_2 - \delta(x_2 - x_1) \\ \dot{y}_2 &= x_2 - k_2 y_2 \end{aligned} \tag{11}$$

4.2 Symmetry properties

Let us consider an autonomous system written in the form:

$$\frac{\boldsymbol{x}}{dt} = \boldsymbol{f}(\boldsymbol{x}), \tag{12}$$

where $\boldsymbol{f} : \boldsymbol{R}^n \to \boldsymbol{R}^n$ is a smooth function for $\boldsymbol{x} \in \boldsymbol{R}^n$. Define a transformation P such as

$$\begin{array}{rcl} P : \boldsymbol{R}^n & \to & \boldsymbol{R}^n \\ \boldsymbol{x} & \mapsto & P\boldsymbol{x} \end{array} \tag{13}$$

If Eq. (12) is invariant under the transformation Eq. (13), i.e.,

$$\boldsymbol{f}(P\boldsymbol{x}) = P\boldsymbol{f}(\boldsymbol{x}) \quad \text{for all } \boldsymbol{x} \in \boldsymbol{R}^n, \tag{14}$$

then the the system (12) is called P-invariant.

Let I_4 is a 4×4 identity matrix. If $k_1 \neq k_2$, only $P = I_4$ and $P = -I_4$ are P-invariant for Eq. (11), i.e., there exists a symmetry group Γ:

$$\Gamma = \{I_4, -I_4\} \tag{15}$$

For $-I_4$ we have an invariant transformation as follows:

$$(x_1, y_1, x_2, y_2) \to (-x_1, -y_1, -x_2, -y_2) \tag{16}$$

This symmetry property directly affects dynamic behavior, for instance, pitchfork bifurcation for equilibria and limit cycles are possibly occurred.

In the case of $k_1 = k_2$, the system has a symmetry as follows:

$$\sigma = \begin{pmatrix} 0 & I_2 \\ I_2 & 0 \end{pmatrix} \tag{17}$$

where, I_2 is a 2×2 identity matrix. Thus the following set Γ_s forms a group.

$$\Gamma_s = \{\sigma, -\sigma, I_4, -I_4\} \tag{18}$$

where, I_4 is an 4×4 identity matrix. For this symmetrical case, the bifurcations of equilibria and limit cycles in Eq. (11) are completely classified with the group theory by Kitajima [Kitajima *et al.*, 1998], however, the case $k_1 \neq k_2$ is not mentioned.

The solution of Eq.(12) is expressed as

$$\boldsymbol{x}(t) = \boldsymbol{\varphi}(t, \boldsymbol{x}_0) \tag{19}$$

and it holds the following initial condition:

$$\boldsymbol{x}(0) = \boldsymbol{x}_0 = \boldsymbol{\varphi}(0, \boldsymbol{x}_0). \tag{20}$$

A limit cycle whose period is L can be written in the form:

$$\boldsymbol{\varphi}(0, \boldsymbol{x}) = \boldsymbol{\varphi}(L, \boldsymbol{x}), \quad L \neq 0. \tag{21}$$

Besides if a limit cycle holds

$$P\boldsymbol{\varphi}(t, \boldsymbol{x}) = \boldsymbol{\varphi}(t, P\boldsymbol{x}) = \boldsymbol{\varphi}(\boldsymbol{x}, t - \tau_P), \tag{22}$$

then we call this solution (P, τ_P)-symmetry limit cycle. For Eq. (11) with $k_1 \neq k_2$, $(-I_4, L/2)$-symmetry limit cycles are frequently generated and they sometimes have the pitchfork bifurcation. New limit cycles after this bifurcation does not preserve $(-I_4, L/2)$-symmetry in this system (symmetry-breaking pitchfork bifurcation).

4.3 Poincaré Mapping for Limit Cycles

To study bifurcation phenomena in Eq.(11), we use the Poincaré mapping method. Assume that Eq. (12) has a limit cycle with period $L > 0$. Without loss of generality, let this limit cycle be the one described by Eq. (20), which passes through the point $\boldsymbol{x}_0$. Then we can define a cross-section, Π, which is transversal to the orbit of the limit cycle, by using a scalar function $q : \boldsymbol{R}^n \to \boldsymbol{R}$:

$$\Pi = \{\, \boldsymbol{x} \in \boldsymbol{R}^n \mid q(\boldsymbol{x}) = 0 \,\}\,, \tag{23}$$

Assume also a periodic solution curve $\boldsymbol{\varphi}(t)$ intersects $\boldsymbol{x}_0 \in Pi$. Since the cross-section is chosen to be transversal to the periodic orbit, we have

$$\frac{\partial q}{\partial \boldsymbol{x}} \cdot \boldsymbol{f} = \boldsymbol{f}(\boldsymbol{x}) \operatorname{grad} q(\boldsymbol{x}_0) \neq 0. \tag{24}$$

Choose a suitable cross-section that is parallel with an orthogonal coordinate frame of $\boldsymbol{R}^n$, and let $\hat{\Pi} \subset \Pi$ be a neighborhood of a point $\boldsymbol{x}$ on the cross-section, and let $\tilde{\boldsymbol{x}} \in \hat{\Pi}$. Then, the Poincaré map, T, is described by

$$T : \hat{\Pi} \to \Pi; \quad \tilde{\boldsymbol{x}} \mapsto \boldsymbol{\varphi}(\tau(\tilde{\boldsymbol{x}}), \tilde{\boldsymbol{x}})\,, \tag{25}$$

where $\tau = \tau(\tilde{\boldsymbol{x}})$ is the return time the orbit travels from point $\tilde{\boldsymbol{x}} \in \hat{\Pi}$ back to Π again (it is coincident to the period L of the limit cycle), then it forms the following discrete system:

$$\boldsymbol{x}_{k+1} = T(\boldsymbol{x}_k). \tag{26}$$

The fixed point of T is given by

$$T(\boldsymbol{x}_0) = \boldsymbol{x}_0. \tag{27}$$

Unfortunately, Eq.(27) cannot be used as a condition to locate $\boldsymbol{x}_0$ since each coordinate value of the fixed point is not independent. This fact affects the convergence ability of Newton's method[Ueta *et al.*, 1997]. To avoid this difficulty, an $(n-1)$-dimensional local coordinate frame, Σ, attached to the cross-section. A projection, $h : \Pi \to \Sigma$, is defined as

$$h : \Pi \to \Sigma \subset \boldsymbol{R}^{n-1}; \quad \boldsymbol{x} \mapsto \boldsymbol{u} = h(\boldsymbol{x}) \tag{28}$$

The induced embedding map is as:

$$h^{-1} : \quad \Sigma \to \Pi \subset \boldsymbol{R}^n; \quad \boldsymbol{x} \mapsto \boldsymbol{x} = h^{-1}(\boldsymbol{u}). \tag{29}$$

Suppose that $\boldsymbol{u}_0 \in \Sigma \subset \boldsymbol{R}^{n-1}$ is located on the local coordinate frame, such that $h(\boldsymbol{x}_0) = \boldsymbol{u}_0$. Also, let $\hat{\Sigma}$ be a neighborhood of $\boldsymbol{u}_0 \in \Sigma$, $\boldsymbol{u}_1$ be a point on $\hat{\Sigma}$ such that $h^{-1}(\boldsymbol{u}_1) = \boldsymbol{x}_1 \in \hat{\Pi}$, and $\boldsymbol{\varphi}(t, \boldsymbol{x}_1)$ be the solution starting from $\boldsymbol{x}_1$. Moreover, suppose that the orbit $\boldsymbol{\varphi}(t, \boldsymbol{x}_1)$ intersects Π at the point $\boldsymbol{x}_2 \in \Pi$ in the return time $\tau(\boldsymbol{x}_1)$, namely,

$$\boldsymbol{x}_2 = \boldsymbol{\varphi}(\tau(\boldsymbol{x}_1), \boldsymbol{x}_1)\,. \tag{30}$$

Then we can define the Poincaré map on the local coordinate frame by

$$\begin{aligned} T_\ell : \quad \hat{\Sigma} &\to \Sigma \\ \boldsymbol{u}_1 \mapsto \boldsymbol{u}_2 &= h(\boldsymbol{\varphi}(\tau(h^{-1}(\boldsymbol{u}_1)), h^{-1}(\boldsymbol{u}_1))) \\ &= h \circ T \circ h^{-1}(\boldsymbol{u}_1)\,. \end{aligned} \tag{31}$$

Finally we have a discrete system derived from Eq. (31):

$$\boldsymbol{u}_{k+1} = T_\ell(\boldsymbol{u}_k). \tag{32}$$

The fixed point $\boldsymbol{u}_0$ is given by

$$T_\ell(\boldsymbol{u}_0) = \boldsymbol{u}_0\,. \tag{33}$$

Stability of the fixed point is governed by the roots of the characteristic equation:

$$\chi(\mu) = \det\left(\frac{\partial \boldsymbol{\varphi}}{\partial \boldsymbol{x}_0} - \mu I_n\right), \tag{34}$$

where I_n is $n \times n$ identity matrix. Then the location of the fixed point $\boldsymbol{u}_0$, the period τ, and the bifurcation parameter value λ are obtained simultaneously with a given multiplier μ by solving the following equations:

$$\boldsymbol{F}_\ell = \begin{pmatrix} T_\ell(\boldsymbol{u}) - \boldsymbol{u} \\ q(\boldsymbol{\varphi}(\tau, h^{-1}(\boldsymbol{u}))) \\ \chi(\mu) \end{pmatrix} = \boldsymbol{0}\,. \tag{35}$$

For calculation of relevant variational equations and some efficient computation of Eq. (35), see Refs. [Kawakami, 1984], [Ueta *et al.*, 1997].

For pitchfork bifurcation of (P, τ_P)-symmetry limit cycles, we simply use

$$\boldsymbol{x}_2 = \boldsymbol{\varphi}(\tau_P(P^{-1}\boldsymbol{x}_1), P^{-1}\boldsymbol{x}_1)\,. \tag{36}$$

instead of Eq. (30), then compute Eq. (35) with $\mu = 1$ or -1.

4.4 Bifurcation of Equilibria

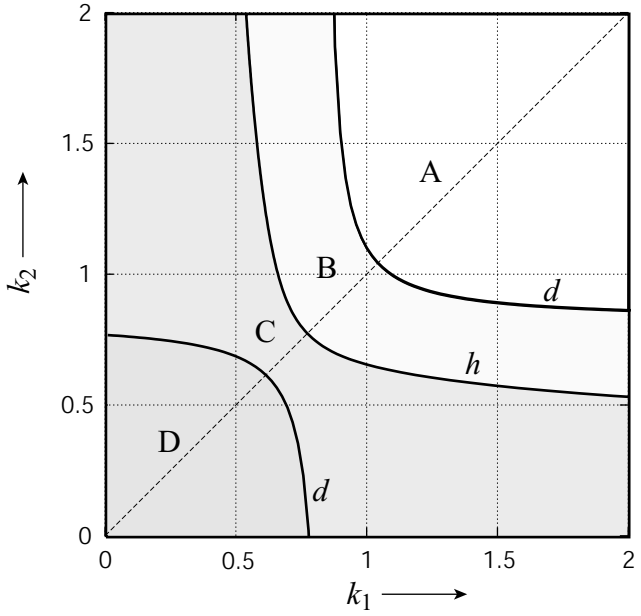

Figure 7: Bifurcation of equilibria

We fix the coupling coefficient as $\delta = 0.337$ ($R = 2000[\Omega]$). Figure 7 shows a bifurcation diagram of equilibria. From the symmetry of k_1 and k_2 in the system, this diagram is symmetrical for $k_1 = k_2$. If a solution $(x_1^*, y_1^*, x_2^*, y_2^*)$ at $(k_1^*,\ k_2^*)$ in this parameter plane is found, also $(x_2^*, y_2^*, x_1^*, y_1^*)$ at $(k_2^*,\ k_1^*)$ is a solution.

In this bifurcation diagram, pitchfork bifurcation curves d for the origin can be obtained analytically as follows:

$$k_2 = \frac{-k_1(\delta - \gamma) - 1}{\delta - \gamma + k_1\gamma(\gamma - 2\delta)}, \tag{37}$$

thus this equation forms hyperbolic curves in k_1-k_2 parameter plane.

At region A, the origin is 2-dimensionally unstable saddle, and there exist sinks $C^+ = (x_{1c}, y_{1c}, x_{2c}, y_{2c})$ and $C^- = (-x_{1c}, -y_{1c}, -x_{2c}, -y_{2c})$. After touching the pitchfork bifurcation curve, i.e., at regions B and C, the origin becomes a 3-dimensionally unstable saddle, and two 1-dimensionally unstable saddles are generated. Similarly, we have 4-dimensionally unstable origin at region D after touching pitchfork bifurcation again.

Getting across region B toward C, above mentioned C^+ and C^- become simultaneously 2-dimensionally unstable saddles by the Hopf bifurcation h. This bifurcation set is solved numerically. Theoretically, two stable limit cycles are generated by this bifurcation, therefore, basically we can roughly conclude that there exist limit cycles in region C and D.

At region D, the origin becomes a completely unstable equilibrium via touching pitchfork bifurcation again.

4.5 Bifurcation of Limit Cycles

Limit cycles would meet several local bifurcations and they exhibit complicated motion. We investigate these bifurcations by using Poincaré mapping method summarized in Sec.4.3.

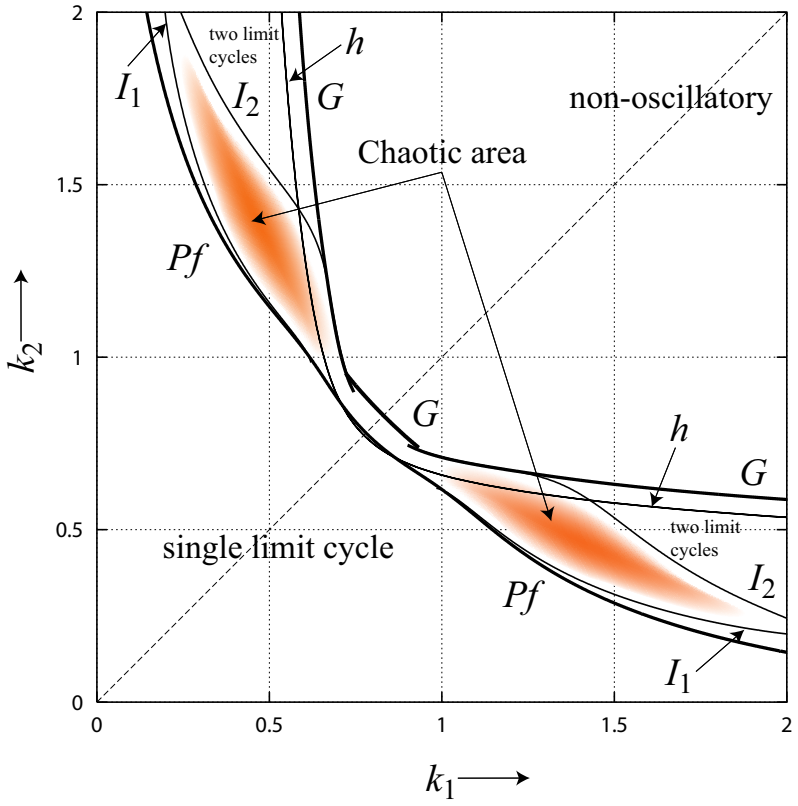

Figure 8: Bifurcation of limit cycles. $\delta = 0.337$.

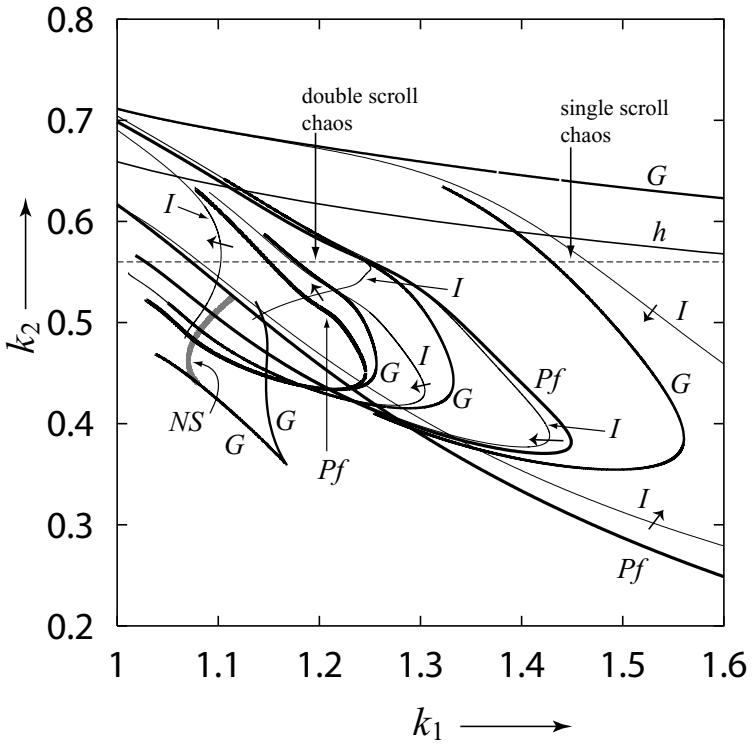

Figure 9: Enlargement of Fig.8

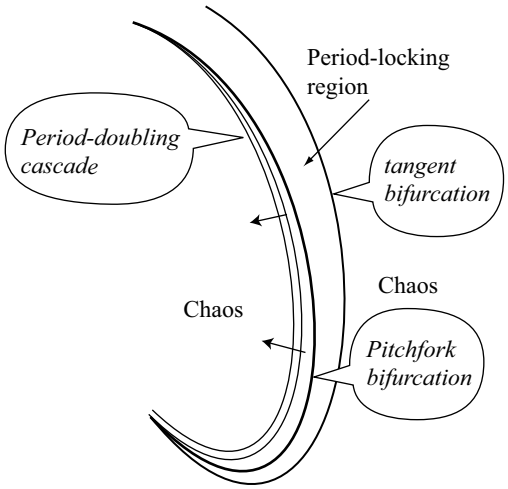

Figure 10: Typical structure of the period-locking area.

4.5.1 Bifurcations in k_1-k_2 Plane

Figure 8 shows a global bifurcation diagram for limit cycles in k_1-k_2 plane with $\delta = 0.337$. Basically this figure can be split into two parts; oscillatory and non-oscillatory regions by the tangent bifurcation G.

In oscillatory region, there exists single $(-I_4, L/2)$-symmetric solution, and it would be bifurcated by crossing the pitchfork bifurcation Pf. Then two stable limit cycles are generated, and they soon meet a period-doubling cascade started from the period-doubling bifurcation I_1.

On the other hand, it is noteworthy that Hopf bifurcation h for C^+ or C^- is not a mandatory condition for generating two limit cycles, in fact, such limit cycles are disappeared by the tangent bifurcation G. So

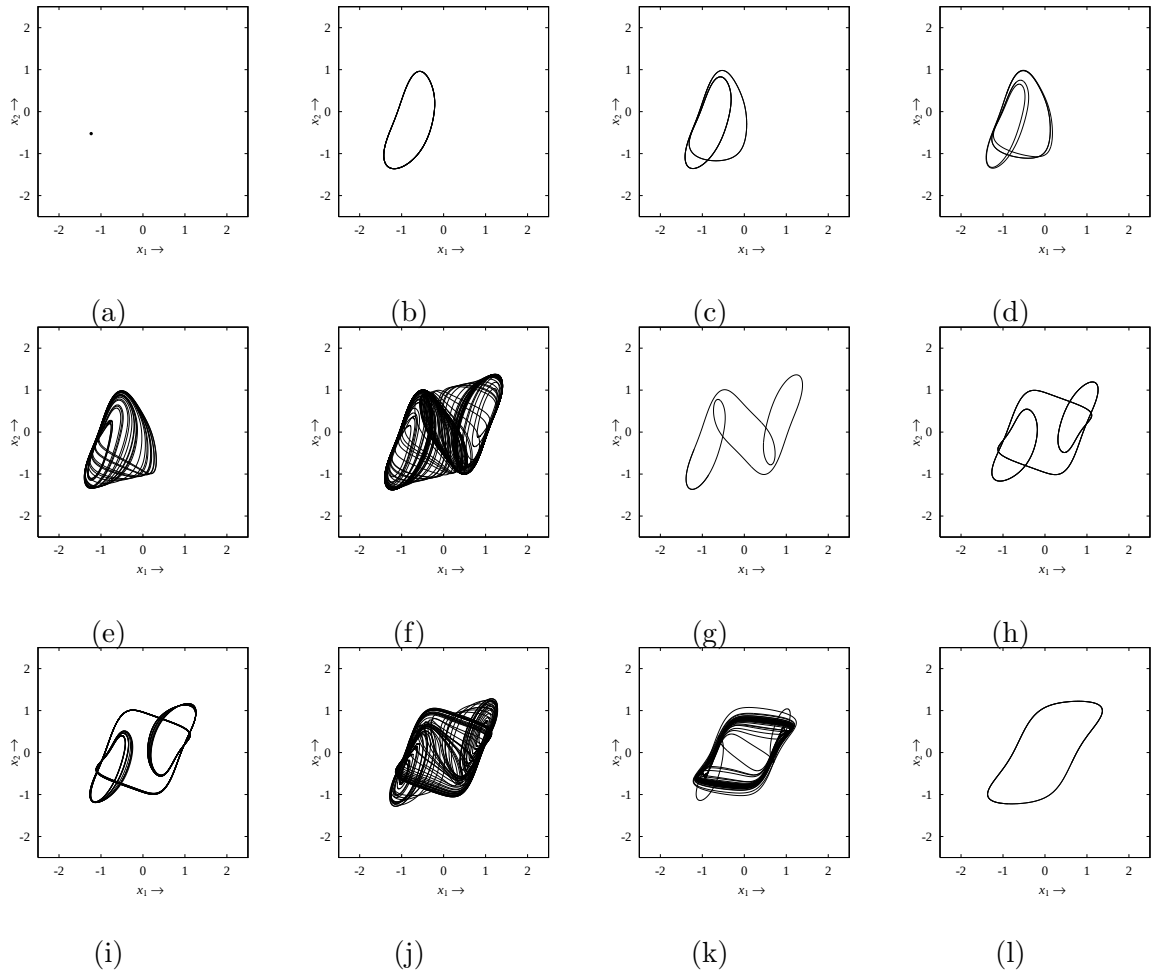

Figure 11: Phase portraits observed along the dotted line in Fig. 9 with $k_2 = 0.56$. (a): $k_1 = 1.51$, (b): $k_1 = 1.461$, (c): $k_1 = 1.451$, (d): $k_1 = 1.441$, (e): $k_1 = 1.43$, (f): $k_1 = 1.248$, (g): $k_1 = 1.245$, (h): $k_1 = 1.24$, (i): $k_1 = 1.112$, (j): $k_1 = 0$.

in the area surrounded by h and G, these cycles survive, thus limit cycles and stable equilibria C^+ and C^- coexist together in this area. These two limit cycles would meet a period-doubling cascade started from I_2. Therefore, the shaded area in Fig.8 can be roughly classified as chaotic areas via period-doubling cascades.

Figure 9 shows an enlargement around the chaotic region shown in Fig.8. There exist many period-locking (window) regions and some of them are depicted. Each regions forms an island and consists of a set of a tangent, pitchfork bifurcations and a period-doubling cascade. This structure is totally different from the Arnold's tongue, or the fish-hook structure. Fig, 10 illustrates a typical structure of the region. In fact, the system has something symmetrical property possesses this type bifurcation structure[Ueta *et al.*, 2000].

Every I forms a period-doubling cascade. In the figure, the direction of the cascade is indicated by small arrows on bifurcation curves I.

Neimark-Sacker bifurcation of a limit cycle is found, however, the torus generated just after this bifurcation cannot survive.

Now we are noticed that no period doubling bifurcation occurred near $k_1 = k_2$. As far as we examined roughly, this situation is not changed even if the coupling coefficient is varied. These observations mean that there exist no chaotic motions in the system coupled by two identical BVP oscillators with reasonable parameter values (6).

4.5.2 Bifurcation Structure and Strange Attractors

Let us fix the parameter k_2 as 0.56. Figure 9 shows a magnification diagram of Fig. 8. Many peninsulas surrounded by bifurcation sets are visualized. Tangent, pitchfork, and period-doubling bifurcations form complex structures on the parameter space.

Let us fix $k_2 = 0.56$, now we explain the bifurcation phenomena by using laboratory experiment results by gradually decreasing k_1 from 1.6 ($r_1 \approx 1100$).

$k_1 \approx 1.5$, there exist two sinks in the space, see Fig.11(a). As mentioned above, a stable limit cycle and a sink coexist together at this parameter value. (bi-stable situation) After touching Hopf bifurcation of these sinks, we surely have two limit cycles, see Fig. 11(b).

Near $k_2 = 0.7$, these limit cycles are bifurcated by period doubling bifurcation cascade; I^i, $i = 1, 2, 4, \ldots, 2^n, \ldots, \infty$. Fig. 11(c) is 2-periodic and Fig. 11(d) is 4-periodic solutions, respectively. Via period doubling cascade, we have a Rössler-type single scroll chaotic attractor, see Figs. 11(e). This type attractor eventually changes to double scroll attractor after the boundary crisis, see Fig. 11(f).

Note that if the coupling is suddenly disconnected, one oscillator stays at a sink and the other one is oscillating itself at this parameter values. Thus an excitatory activity and a resting activity give this strange attractor by the coupling term.

Period-locking areas as windows are embedded in the chaotic region. The starting edge of the region is the tangent bifurcation G, and the solution just after touching this bifurcation is $(-I_4, L/2)$-symmetric solution, see Fig. 11(g). Every pitchfork bifurcation curve Pf affects this symmetric solution as a symmetry-breaking branching, i.e., after this bifurcation, two periodic solutions are generated, and they are not $(-I_4, L/2)$-symmetry. Such solutions soon meet a period-doubling cascade, see Fig. 11(i), and finally they are merged and form double scroll attractor, see Fig.11(j).

Around $k = 1.112$, the double scroll is decomposed and shrieked into single $(-I_4, L/2)$-symmetry attractor, see Fig.11 (k) and (l).

We confirm this bifurcation phenomena in the laboratory experiment. All attractors shown in Fig. 11(a)–(l) are realized in a circuitry with a good accuracy, see Fig. 12.

We assert that chaotic behavior is almost brought by period-doubling bifurcation cascades. As a numerical confirmation of chaos, we show Fig. 13. This depicts all Lyapunov exponents along dash line in Fig. 9. It is visualized that the positive exponent indicates the chaotic behavior. Also typical variation can be visualized in this figure, i.e., alternatively zero-touching of the maximum exponent according to

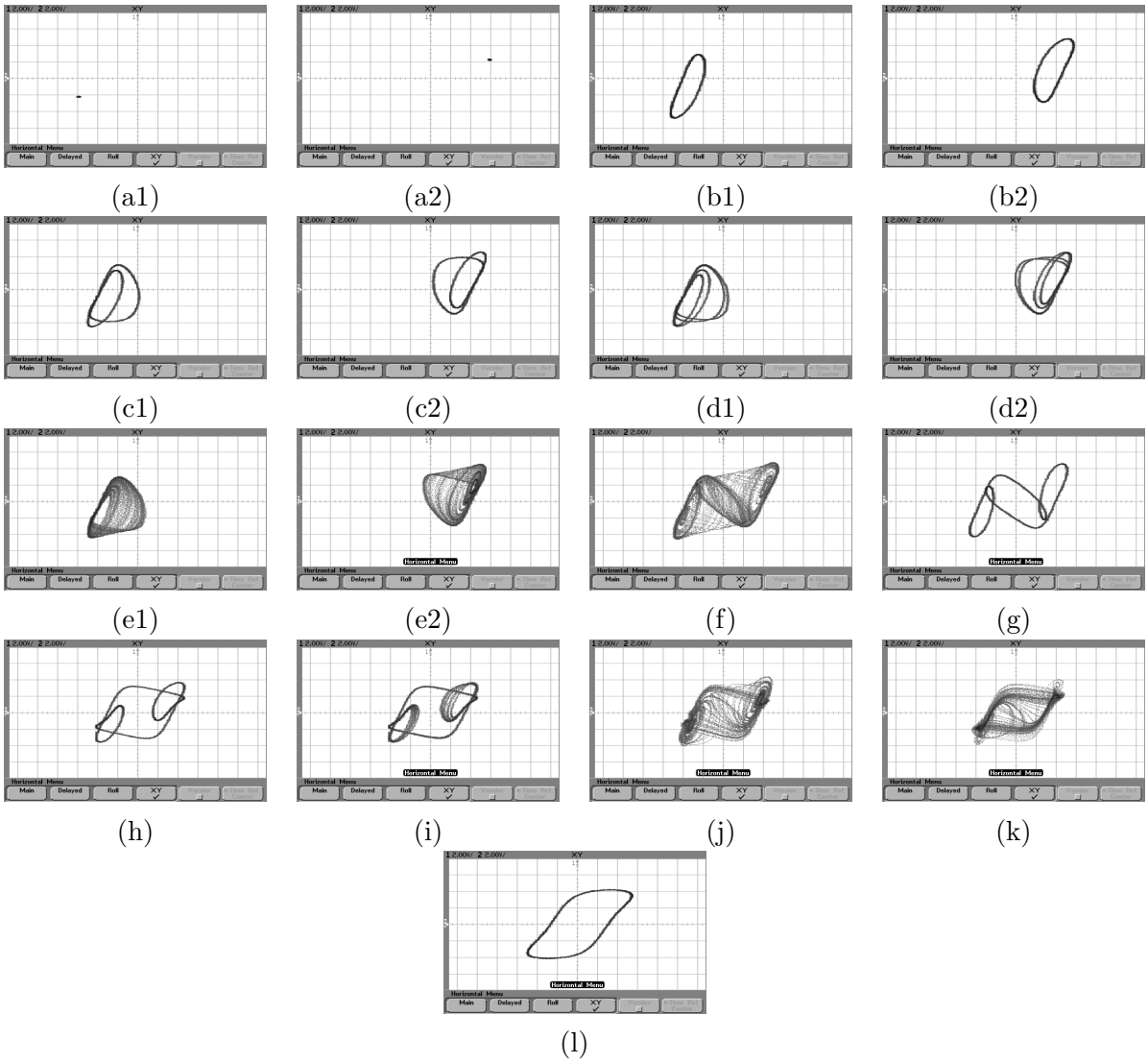

Figure 12: Laboratory experiments according to the simulation Fig. 11 by gradually decreasing r_1. (a): sinks, (b): limit cycles via Hopf bifurcation, (c)–(e): the period-doubling cascade, (f), (j), (k): double scroll, (g) $(-I_4, L/2)$-attractor. (i)–(j) asymmetric attractor just after the pitchfork bifurcation and its chaos, (l) a simple $(-I_4, L/2)$-attractor.

period-doubling bifurcations, fractures of negative exponents in chaotic region as 'window' regions.

Now we decrease k_2 as 0.45. Figure 14 shows also an enlargement of Fig.8. It visualized I^2, which shows period-doubling of 2-periodic limit cycles. Figures 15 and 16 show various attractors, and Figure 17 shows all Lyapunov exponents along the dash line in Fig.14. We assure that the approximation of FET and the mathematical model Eq. 11 are very accurate from these results.

Figure 18 shows various information of the typical strange attractor in two dimensional phase space, wave forms, the Ponicaé mapping. It looks like double scroll attractor[Chua *et al.*, 1986], and it is impressive because a couple of BVP oscillators can exhibit such complicate response. Figure 19 shows a three dimensional structure of the attractor. There exist some constrain planes in the space and single positive Lyapunov exponent explains such dissipative, 'thin' chaotic attractor. Poincare mappings Figs 18(c) and 20 (f) characterized this attractor.

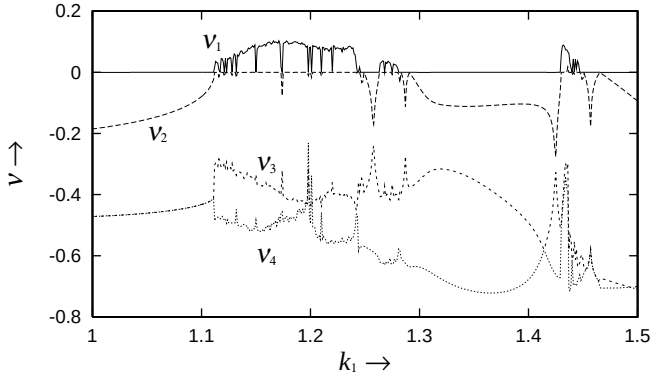

Figure 13: Lyapunov exponents. $k_2 = 0.56$.

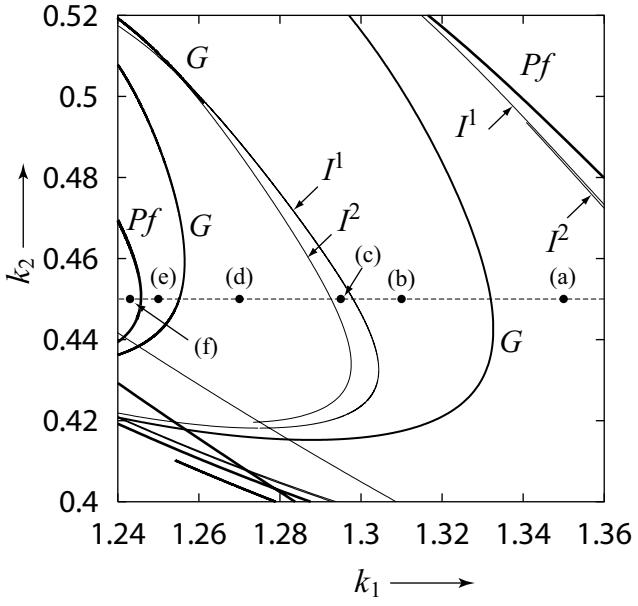

Figure 14: Enlargement of Fig.8

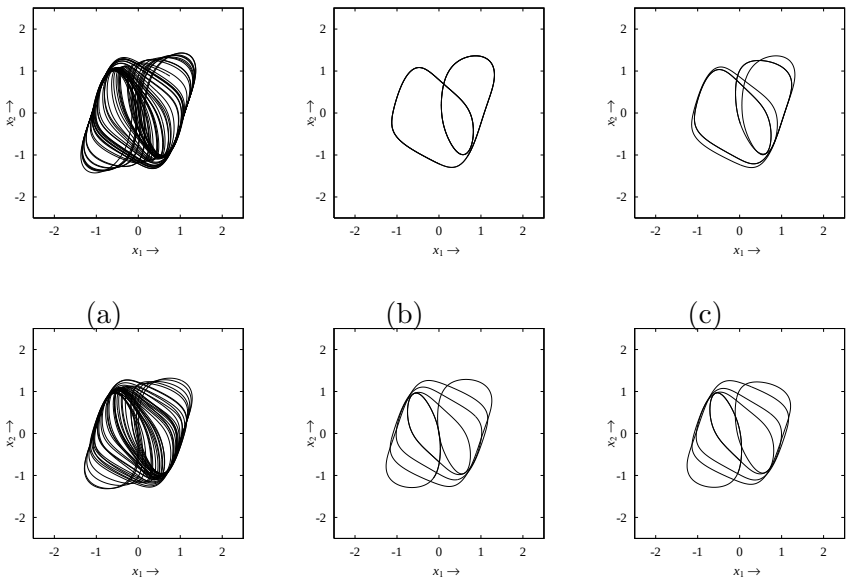

Figure 15: Phase portraits in x_1-x_2 plane. $k_2 = 0.45$. (a): $k_2 = 1.35$, (b): $k_2 = 1.31$, (c): $k_2 = 1.295$, (d): $k_2 = 1.27$, (e): $k_2 = 1.25$, (f): $k_2 = 1.243$. Fig. (f) is given by a pitchfork bifurcation of $(-I_4, L/2)$ solution shown in Fig. (e).

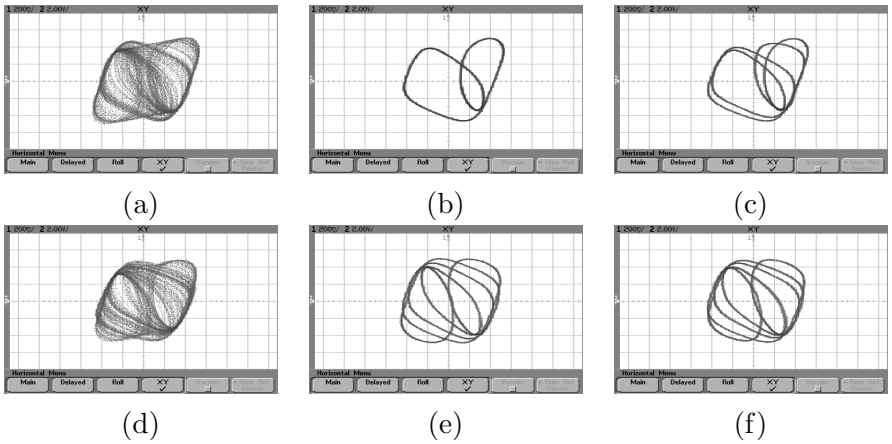

Figure 16: Laboratory experiments in v_1-v_2 plane according to Fig. 15.

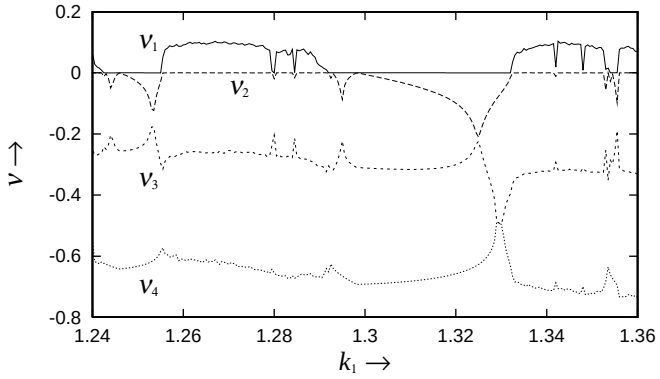

Figure 17: Lyapunov exponents. $k_2 = 0.45$.

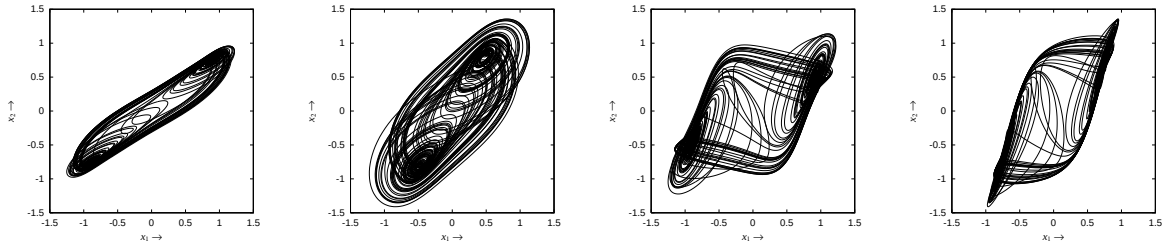

(a) x_1-y_1, (b) x_2-y_2 (c) x_1-x_2, (d) y_1-y_2

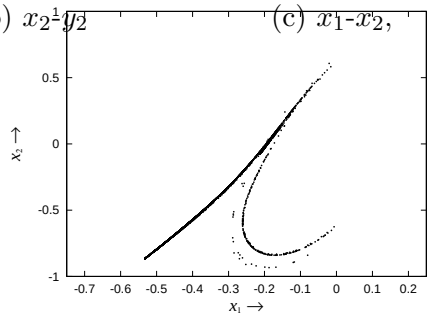

(e) Poincaré mapping at x_1-x_2, $y_1 = 0$.

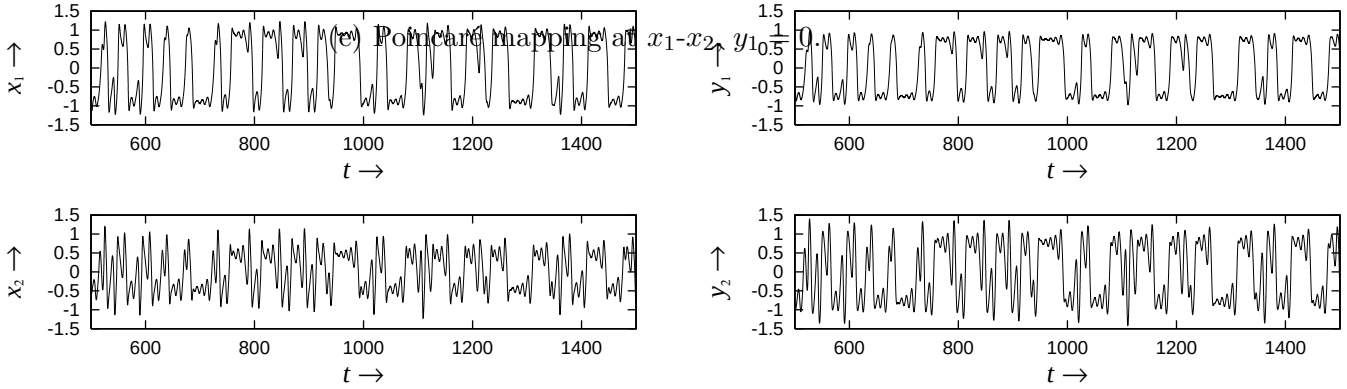

(f) Time responses.

Figure 18: Chaotic attractor. $\delta = 0.337$, $k_1 = 1.187$, $k_2 = 0.593$, ($R \approx 2000[\Omega]$, $r_1 \approx 400[\Omega]$, $r_2 \approx 800[\Omega]$).

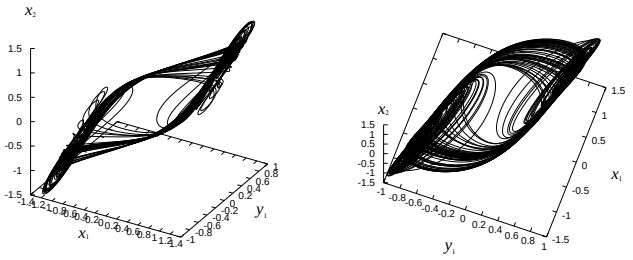

Figure 19: Three dimensional structure of the strange attractor shown in Fig. 18.

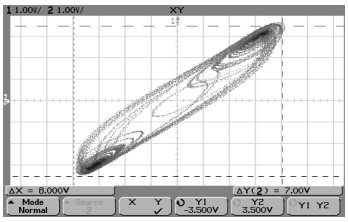

(a) v_1-$r_1 i_1$.

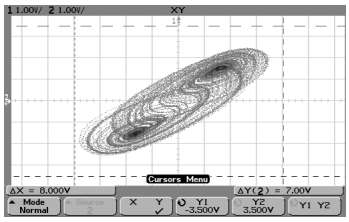

(b) v_2-$r_2 i_2$.

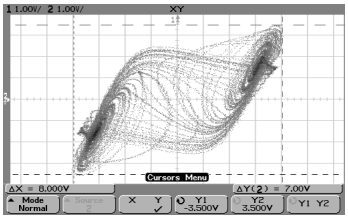

(c) v_1-v_2.

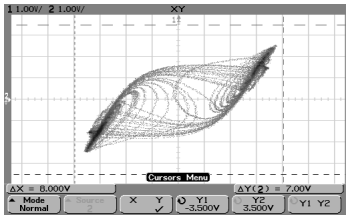

(d) $r_1 v_1$-$r_2 i_2$.

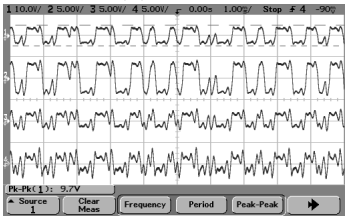

(e) Wave forms. v_1, $r_1 i_1$, v_2, $r_2 i_2$

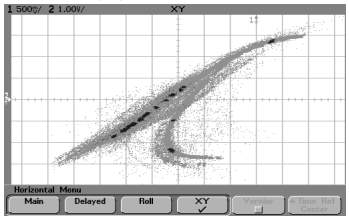

(f) Poincaré mapping on v_1-v_2. $i_1 = 0$.

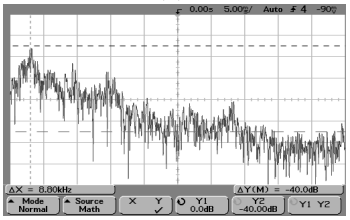

(g) Frequency components.

Figure 20: Typical strange attractor. $R \approx 2000[\Omega]$, $r_1 \approx 780[\Omega]$, $r_2 \approx 380[\Omega]$. Poincaré mapping contains noise which comes from switching action of the S/H chip.

4.6 Dependency of δ

Now we should mention choice of the coupling coefficient. Let us fix $k_2 = 0.56$. Figure 21 shows a global bifurcation diagram in δ-k_1 plane, and Fig. 22 shows its enlargement. There exist basically three regions which contain two limit cycles, non-oscillation, and single limit cycle, respectively. These regions are sectioned by bifurcation curves. There exist a chaotic region via period-doubling cascades in the center part of these figures.

These figures imply that the choice of δ in previous sections is a suitable parameter value because many variations of bifurcations are contains along $\delta = 0.337$. Also we notice that the both parameter ranges $\delta > 0.8$ and $\delta < 0.2$ simplify the system behavior.

In Fig.22, complicated structures of period-locking area in chaotic region are indicated. Small arrows also visualized the direction of progress of the period-doubling cascade. The double scroll attractors appears within these chaotic regions.

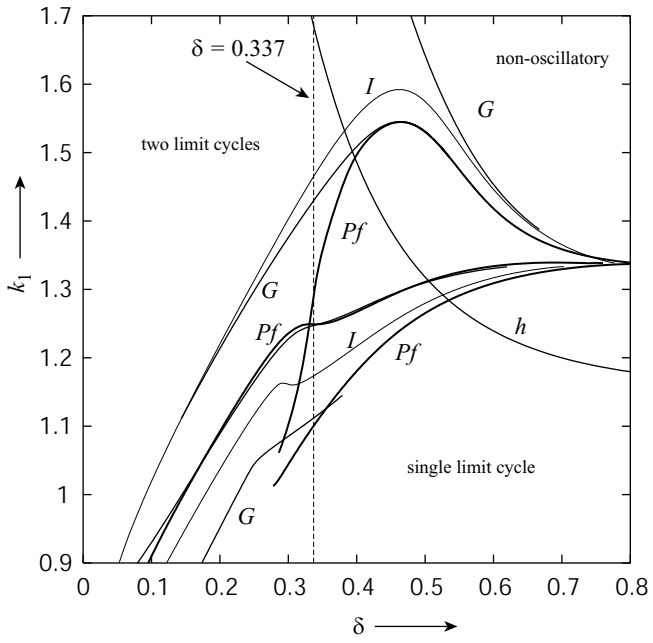

Figure 21: Bifurcation diagram in δ-k_1 plane. $k_2 = 0.56$.

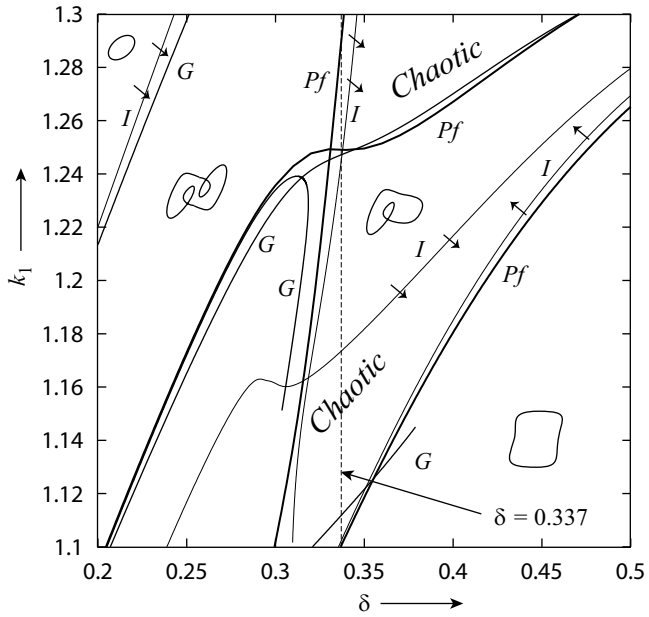

Figure 22: Enlargement of Fig. 21. The small arrows indicate the direction of progress for period-doubling cascades.

4.7 Third-Power Term Nonlinearity

In fact, the saturation (sigmoid) characteristics in Eq. (2) is not necessary for generation of double scrolls such as Fig. 18. Instead of this characteristics, one can use a cubic function $g(v) = ax + bx^3$.

In Sect. 4.5, all attractors are almost in $-4 < v_i < 4$ [V] range. In this interval, the third-power approximation is applicable. In fact, for the range ± 4[V], the result of the fitting method gives:

$$a = -2.27255 \times 10^{-3}, \quad b = 4.71518 \times 10^{-5}, \tag{38}$$

and Fig. 23 shows the shape of the approximated function.

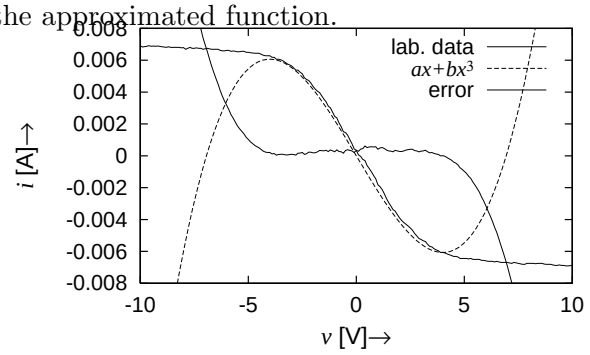

Figure 23: Measurement data of the FET, its approximation by a third-power polynomial, and the error between them.

Let state variables and parameters be

$$x_j = \frac{C}{\sqrt{b\sqrt{\frac{L}{C}}}} v_j, \quad y_j = \sqrt{\frac{\frac{L}{C}}{b\sqrt{\frac{L}{C}}}} i_j, \tag{39}$$

$$k_j = r_j \sqrt{\frac{C}{L}}, \qquad j = 1, 2.$$

$$\tau = \frac{1}{\sqrt{LC}} t, \quad \gamma_3 = a\sqrt{\frac{L}{C}} \quad \delta = \sqrt{\frac{L}{C}} G. \tag{40}$$

Thus we have the following simple equations:

$$\begin{aligned} \dot{x}_1 &= -y_1 + \gamma_3 x_1 + x_1^3 - \delta(x_1 - x_2) \\ \dot{y}_1 &= x_1 - k_1 y_1 \\ \dot{x}_2 &= -y_2 + \gamma_3 x_2 + x_2^3 - \delta(x_2 - x_1) \\ \dot{y}_2 &= x_2 - k_2 y_2 \end{aligned} \tag{41}$$

Figure 24 shows a global bifurcation diagram of Eq. (41) corresponding to Fig. 8. All bifurcation curves found in Fig. 8 are preserved in Fig. 24. Period-doubling cascades and other many bifurcation sets are also found inside of the area surrounded by I_1 and I_2. With a reasonable parameter set, we have a topologically similar chaotic attractor compared with Fig. 20, see Fig. 25. Therefore, it can be concluded that the third-power nonlinearity contributes drastically to the conspicuous chaotic behavior, and Eq. 2 is suitable as a $g(v)$ for the BVP oscillator.

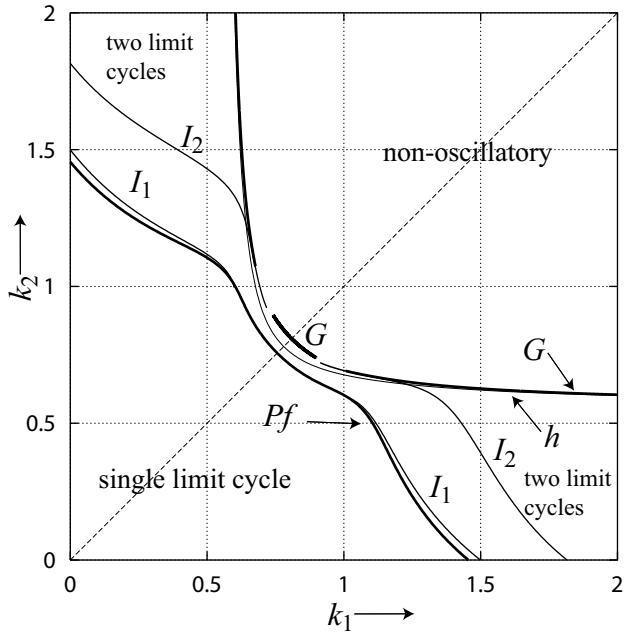

Figure 24: Bifurcation diagram of Eq. (41), $\gamma_3 = 1.53165$, $\delta = 0.337$.

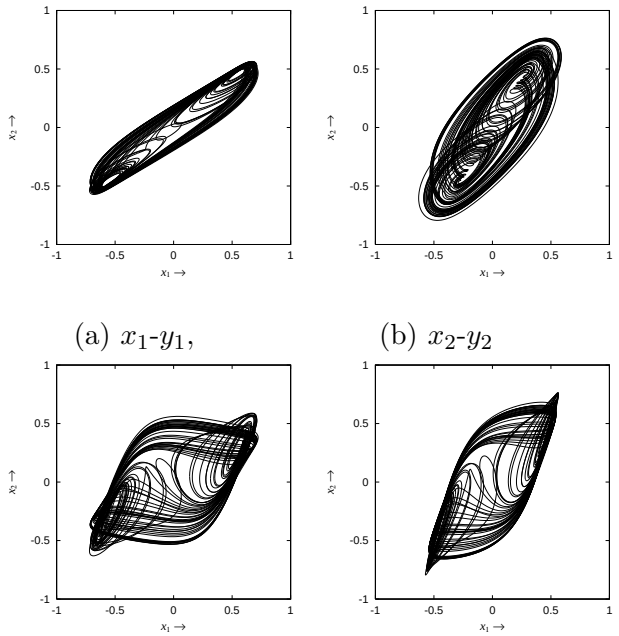

(a) x_1-y_1, (b) x_2-y_2

(c) x_1-x_2, (d) y_1-y_2

Figure 25: Chaotic attractor. $\gamma_3 = 1.53165$. $k_1 = 1.127$, $k_2 = 0.638$, $\delta = 0.337$.

5 Conclusions

We investigated bifurcation phenomena and strange attractors in the resistively coupled BVP oscillators. A rich variety of bifurcations and chaotic attractors are obtained by changing parameters. To analyze dynamical properties of the system, we calculate bifurcation diagrams by using the Poincaré mapping

method. Bifurcation structure and chaotic parameter regions are clarified in the parameter space.

Since each oscillator has different value of internal resistance, chaotic behavior is obtained as a compromise of activities from two different oscillators; a conspicuous strange attractor is obtained.

As the future problems,

- to clarify bifurcations of equilibria of Eq.(11).
- to investigate other parameter values, especially, R and C, L.
- to investigate synchronization phenomena of limit cycles and chaos when a large number BVP oscillators are coupled.

References

[FitzHugh, 1961] FitzHugh, R. "Impulses and Physiological States in Theoretical Models of Nerve Membrane," Biophys. J., Vol. 1, pp.445–466, 1961.

[Nagumo, 1962] Nagumo, J., Arimoto, S. and Yoshizawa, S., "An Active Pulse Transmission Line Simulating Nerve Axon," Proc. IRE, Vol. 50, No. 10, pp. 2061–2070, 1962.

[Hodgkin *et al.*, 1952] Hodgkin A. L. and Huxley A. F., "A Qualitative Description of Membrane Current and its Applications to Conduction and Excitation in Nerve," J. Physiol., Vol. 117, pp. 500–544, 1952.

[Rocsoreanu *et al.*, 2000] Rocsoreanu C., Georgescu A., Giurgiteanu, N., The FitzHugh-Nagumo Model Bifurcation and Dynamics, Mathematical Modeling: Theory and Applications, Vol. 10, Kluwer Academic Publishers, Dordrecht, 2000.

[Bautin, 1975] Bautin, A. N., "Qualitative Investigation of a Particular Nonlinear System," Journal of Applied Mathematics and Mechanics, vol. 39, No. 4, pp. 606–615, 1975.

[Kitajima *et al.*, 1998] Kitajima, H. Katsuta Y. and Kawakami H., "Bifurcations of Periodic Solutions in A Coupled Oscillator with Voltage Ports," IEICE Trans. Fundamentals, Vol. E81-A, No.3, pp.476-482, 1998.

[Linkens, 1974] Linkens, D. A., "Analytical Solution of Large Numbers of Mutually Coupled Nearly Sinusoidal Oscillators," IEEE Trans. Circuits and Systems, Vol. CAS-21, No.2, pp.294–300, 1974.

[Endo *et al.*, 1978] Endo, T. and Mori, S., "Mode Analysis of a Ring of a Large Number of Mutually Coupled van der Pol Oscillators," IEEE Trans. Circuits and Systems, Vol. CAS-25, No. 1, pp.7–18, 1978.

[Hoque *et al.*, 1995] Hoque M. and Kawakami, H., "Resistively Coupled Oscillators with Hybrid Connection," IEICE Trans. Fundamentals, Vol. E78-A, No. 9, pp.1253–1256, 1995.

[Papy *et al.*, 1995] Papy O. and Kawakami H., "Symmetrical Properties and Bifurcations of the Periodic Solutions for a Hybridly Coupled Oscillator," IEICE Trans. Fundamentals, Vol. E78-A, No. 12, pp.1816–1821, 1995.

[Papy *et al.*, 1996] Papy O. and Kawakami H., "Symmetry Breaking and Recovering in a System of n Hybridly Coupled Oscillators," IEICE Trans. Vol. E79-A, No. 10, pp. 1581-1586, 1996.

[Tsumoto *et al.*, 1999] Tsumoto, K., Yoshinaga T., and Kawakami, H., "Bifurcation of a Modified BVP Circuit Model for Neurons Generating Rectangular Waves," IEICE Trans. Fundamentals, Vol. E82-A, No.9, pp.1729–1736, 1999.

[Chua *et al.*, 1986] Chua, L. O., Komuro, M., and Matsumoto, T., "The Double Scroll Family," IEEE Trans. Circuits and Systems, Vol. CAS-33, pp.1073-1118, 1986.

[Chua, 1993] L. O. Chua, "Global Unfolding of Chua's Circuit," IEICE Trans. Vol. 76-A, No. 5, pp. 704–734, 1993.

[Kawakami, 1984] Kawakami, H., "Bifurcation of Periodic Responses in Forced Dynamic Nonlinear Circuits: Computation of Bifurcation Values of the System Parameters," IEEE Trans. Circuits and Systems, Vol. CAS-31, No. 3, pp.246–260, 1984.

[Ueta *et al.*, 1997] Ueta, T., Tsueike M., Kawakami, H., Yoshinaga T., and Katsuta, Y., "A Computation of Bifurcation Parameter Values for Limit Cycles," IEICE Trans. Fundamentals, Vol. E80-A, No. 9, pp. 1725-1728, 1997.

[Ueta *et al.*, 2000] Ueta T. and Chen, G., "Bifurcation Analysis of Chen's Equation," International Journal of Bifurcation and Chaos, Vol. 10, No. 8, pp. 1917-1931, 2000.